ELSEVIER

Biochimica et Biophysica Acta 1507 (2001) 80–99

BIOCHIMICA ET BIOPHYSICA ACTA

BBA

www.bba-direct.com

Review

Energy transfer and trapping in photosystem I

Bas Gobets, Rienk van Grondelle *

Division of Physics and Astronomy, Faculty of Exact Sciences and Institute of Molecular Biological Sciences, Vrije Universiteit, De Boelelaan 1081, 1081 HV Amsterdam, The Netherlands

Received 16 January 2001; received in revised form 6 June 2001; accepted 18 June 2001

Keywords: Photosystem I; Excitation energy transfer; Trapping; Time-resolved fluorescence; Target analysis

1. Introduction

The primary processes in all photosynthetic systems involve the absorption of energy from (sun) light by chromophores in a light harvesting antenna, and the subsequent transfer of this energy to a reaction centre (RC) site where the energy is 'trapped' by means of a stable charge separation.

Photosystem (PS) I is one of two such photosystems in oxygenic photosynthesis. When co-operating with PS II it uses the energy of light to transfer electrons from plastocyanin or soluble cytochrome c_6 to ferredoxin and eventually to $NADP^+$. In an alternative pathway, the electrons from ferredoxin are transferred back to plastocyanin via the cytochrome b_6f complex. This cyclic electron transport, which does not require the input of free energy by PS II, results in a transmembrane electrochemical gradient that can be used to produce ATP.

In plants and green algae the PS I complex consists of two separable functional units: the PS I core, and the light harvesting complex (LHC) I peripheral antenna. The PS I complex in cyanobacteria does not possess the peripheral LHCI antenna, but since the PS I core complexes of cyanobacteria bear a large resemblance to the core complex of plants, a direct comparison of the energy transfer and trapping properties of these complexes is justified [1,2].

2. Basic features of the PS I complexes

2.1. PS I core

The PS I core is a large pigment–protein complex consisting of 11–13 protein subunits [3], the largest two of which, PsaA and PsaB, form a heterodimer to which the majority of the core antenna pigments, as well as most of the reaction centre co-factors are bound. Spectroscopic data indicate that the core antenna and reaction centre contain approx. 90–100 chlorophyll (chl) *a* and 10–25 β-carotene molecules in total.

The PS I core complexes of cyanobacteria can be isolated both as monomers and trimers, which are both equally efficient in energy transfer and charge separation [4]. It is not fully clear which one is the native conformation, although it is very likely that a dynamic equilibrium exists between monomers and trimers in the membrane, which can be regulated by, for instance, the salt concentration [5]. In contrast, plant PS I core complexes do not assemble as trimers, although the peripheral LHCI antenna does not cause structural hindrances for the type of trimerization as observed in cyanobacterial PS I [6].

The structure of the PS I core complex of the

* Corresponding author. Fax: +31-20-444-7899.
E-mail address: rienk@nat.vu.nl (R. van Grondelle).

PII: S0005-2728(01)00203-1

cyanobacterium *Synechococcus elongatus* has been resolved up to 4 Å resolution [7–9], and will be discussed below in terms of its energy transfer capacity.

2.2. Light harvesting complex I

The peripheral LHCI antenna complex of plants is composed of four different proteins, Lhca1–4, which have molecular masses ranging from 20 to 24 kDa, and which are thought to be present in approximately equal amounts [10]. The Lhca1–4 proteins, which bind on the average 8 chl*a*, 2 chl*b* and 2 carotenoid molecules [11,12], assemble as dimers. Lhca1 and Lhca4 have been shown to form a heterodimer [13,14] which exhibits a red shifted low temperature steady-state emission maximum at 730 nm [10], and which has therefore been designated LHCI-730.

Biochemical data suggest that Lhca2 and Lhca3 assemble as homodimers rather than as heterodimers [13]. The 77 K fluorescence of these complexes is usually reported to peak at 680 nm, and therefore they so far have been designated LHCI-680 [10]. It has recently been suggested, however, that LHCI-680 represents monomeric Lhca2 and Lhca3, degradation products of the dimers, which represent the functional complexes in vivo [15]. This idea is further corroborated by recent low temperature (5 K) spectroscopy experiments on a mixture of dimers of Lhca1–4 that, in addition to the 730 nm emission, demonstrate the presence of an emission band at ~702 nm (F702), possibly due to Lhca2/Lhca3 homo/heterodimers [12].

The pigment stoichiometry of LHCI is very similar to that found for CP29, one of the minor antenna proteins of PS II. The LHCI proteins show a large sequence homology to CP29 as well as to other plant light harvesting proteins [10], such as LHCII, which is presently the only Lhca/b protein for which a high resolution (3.4 Å) structure exists [16]. It may therefore be speculated that the general fold of LHCI resembles that of LHCII and the model proposed for the pigment organization in CP29 may also be applied to LHCI [17].

2.3. PS I-200

In plants 3–4 [6] or possibly five [11] LHCI dimers bind to a PS I core particle to assemble into a complex which contains a total of 170–200 chls and which is designated PS I-200. Earlier results suggested that these LHCI dimers completely surround the core [18]. More recent electron microscopy data indicate, however, that all LHCI dimers are located on one side of the core complex. [6].

2.4. Structure of the PS I core

In the 4 Å structure of the PS I core complex of the cyanobacterium *S. elongatus* 89 chl molecules were identified so far, including the 6 chl*a* molecules of the electron transfer chain [7–9]. These chlorophyll sites are shown in Fig. 1, in which the direction of view is perpendicular to the membrane plane. The porphyrin rings which are shown in Fig. 1 indicate the planes in which the rings lie, rather than the exact orientation, which could not be derived from the 4 Å structure.

The RC, i.e. those chlorophylls and cofactors involved in primary electron transfer, is located in the centre of the structure, bound between PsaA and PsaB. The two parallel oriented chls, which are located in the middle of the structure, constitute the primary electron donor P700. The pairs of chls which are located on both sides in the direct vicinity of P700 represent the primary electron acceptor, A_0, and the accessory chls. Also other components of the electron transfer chain, including three Fe_4S_4 iron–sulphur clusters F_x, F_A and F_B, could be assigned in the structure. The location of the two phylloquinones, which constitute A_1, was determined by combining the structural data with single crystal EPR results [19,20].

The remaining 83 core antenna chls are found to be arranged in a more or less elliptically shaped bowl-like structure surrounding the reaction centre. The distance of most antenna chls to any of the RC chls is found to be larger than 20 Å. However, two antenna chls located at ~14 Å from the closest RC pigments stand out in the structure, forming a structural, and possibly functional bridge between the other antenna chls and the RC.

Previously, in the absence of a structure, the modelling of the energy transfer dynamics in PS I was often based on square or cubic lattices [21–24]. For a given configuration, these models generally involve

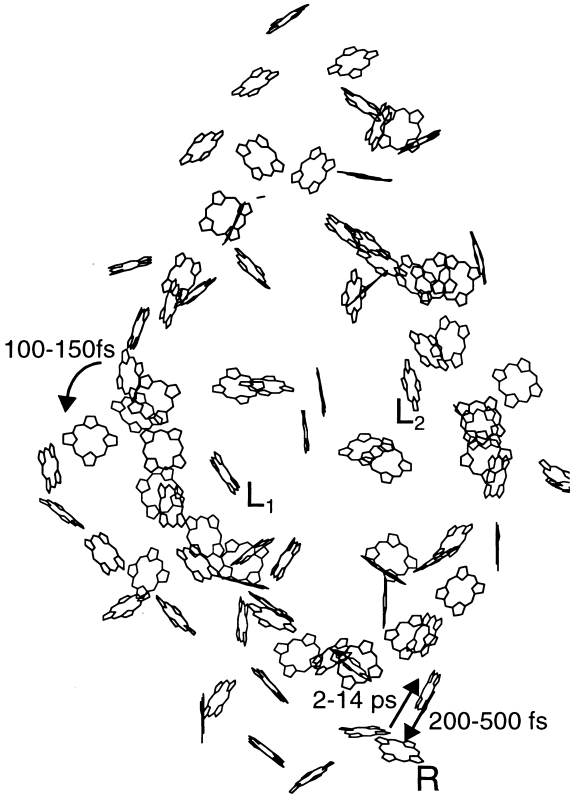

Fig. 1. Positions of chls in PS I as found in the 4 Å structure. The porphyrin rings indicate the plane of the chls rather than the exact orientation in the plane. L_1 and L_2 indicate the proposed 'linker' chls. The indicated rates were calculated as described in the text. R represents a hypothetical red chl.

two separate rates: the energy transfer ('hopping') rate between two sites, and the intrinsic trapping rate from a site representing the primary electron donor P700. This has led to two limiting cases for the dynamics in PS I. In the first, the transfer limited case, the energy transfer rate determines the decay of the excited state due to trapping, while in the second, the trap limited case, the intrinsic rate of charge separation from P700 governs these dynamics. The structure in Fig. 1 shows, however, that the primary electron donor, P700, is not just another site on a lattice. The distance between P700 and the antenna chls is significantly larger as compared to the distance between adjacent antenna chls. Therefore a model describing the energy transfer in PS I should include (at least) two energy transfer rates instead of one: a high rate between the antenna chls, and a lower rate from the antenna to the reaction centre. This leads to a third limiting case; the so-called transfer-to-the-trap limited case, in which the energy transfer from the antenna to the RC is limiting the overall dynamics [25]. Such a model, in which two distinctly different distance scales appear, was already proposed before the availability of the structure, based upon an analogy with the arrangement in purple bacteria [26,27] in which the bacterial RC is surrounded by the LHI ring. Such a ring-like organization of the antenna around the RC appears to be a common feature in photosynthesis. It can easily be shown that such an organization is a prerequisite for an efficient photosystem including a bulky reaction centre. A system in which the RC is located in the centre of a ring-like structure, with a relatively large average distance to each antenna chl, but in contact with many of them collects excited state energy much more efficiently than a system in which the RC would be located at the periphery of the antenna to which it is linked by only a few antenna chls.

3. Low energy ('red') chlorophylls

Both the photosystem I core and the peripheral LHCI antenna are spectrally highly heterogeneous, as can be seen clearly from Fig. 2 in which the low temperature (6 K) absorption spectra of the Q_y region of a number of PS I core complexes, LHCI and PS I-200 are displayed. The major part of the core antenna chlorophylls, which we refer to as 'bulk' chls, absorb in a broad band which shows a maximum at 680 nm. This has to be compared to the absorption profile of isolated chl*a* which displays a single broad maximum at $\sim$670 nm in organic solvents [28]. The low temperature absorption spectra (Fig. 2) clearly exhibit shoulders both on the blue and the red flanks [29–34,4]. An even more striking feature of all (intact) PS I complexes is the presence of a relatively small number of red shifted chlorophylls that absorb at energies lower than that of the primary electron donor P700. Although the number of these low energy chls is small, 3–10% of the total number of chls, they have a very pronounced effect on the energy transfer and trapping in the whole PS I system, which is evident from both time resolved and steady-state spectroscopy experiments. The function of these red chls and the nature of their

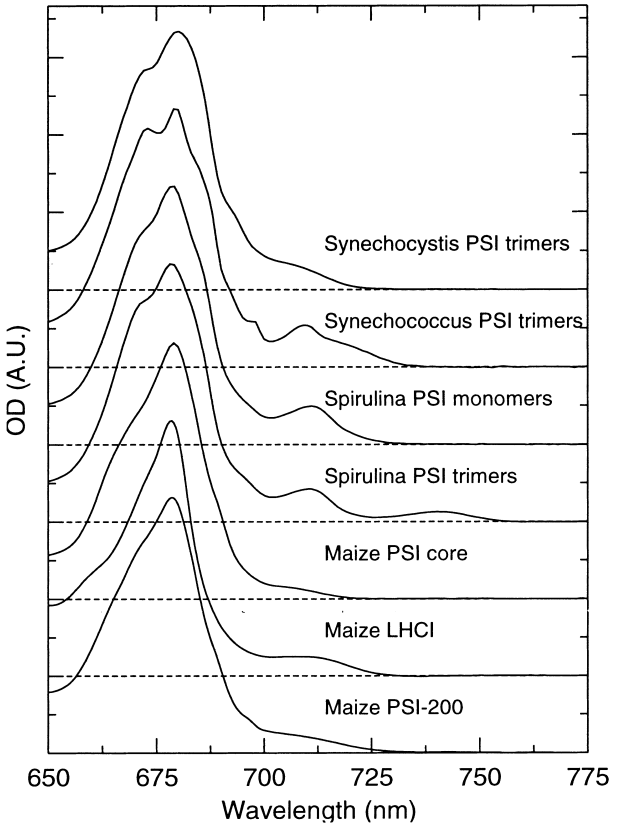

Fig. 2. 6 K absorption spectra of various cyanobacterial PS I cores and the different plant PS I complexes.

extreme red shift are some of the key issues in the spectroscopy of PS I.

3.1. Properties of the red chl pools

3.1.1. Red chls in cyanobacterial PS I cores

In PS I cores of cyanobacteria, the amounts and energies of the low energy chls appear to be highly species dependent. [29–31,33,35] (see Fig. 2). Moreover, the red chl forms are also affected by the aggregation state of the cyanobacterial core complexes: in monomeric PS I core preparations the number of red chls is generally found to be lower than in trimers. Especially the amplitude of the most red shifted chl band may depend strongly upon the aggregation state, which is easily observed upon comparison of the 6 K absorption spectra of isolated monomeric and trimeric PS I from *Spirulina platensis* (spectra 3 and 4 in Fig. 2). It has been shown that upon trimerization of isolated monomers of *Sp. platensis* the trimer red chl absorption emerges [36], indicating that the difference between monomers and trimers is not so much the actual loss of chls in the monomers, but rather that the red shift is due to an interaction induced by trimerization. This effect suggests that these red chls are located in the periphery of the PS I core, in the region where the monomers within the trimer are in contact [37].

Since the absorption bands of red chls are quite distinct at 4 K, the maxima of these bands and the number of chls contained in them can be estimated by Gaussian decomposition of the absorption spectra (Table 1). For trimeric PS I core particles from the cyanobacterium *Synechocystis* PCC 6803 (Fig. 2, spectrum 1) this procedure reveals an inhomogeneously broadened absorption band with a maximum at 708 nm (C708) which carries an oscillator strength of 4–5 chl*a* molecules [38]. Hayes et al. [39], however, have suggested, on the basis of hole burning experiments, that 2 chls contribute to C706, and another 2 chls contribute to C714. We, however, do not find any spectroscopic evidence for the presence of two distinct pools of red chls in the PS I core of *Synechocystis*. The low temperature absorption spectra of *Synechocystis* PS I displayed in Fig. 2 do not show any structure in the red tail. Also in the analysis [38] of our time resolved streak camera data nothing hints at a heterogeneity of the red chls in *Synechocystis* PS I. We therefore favour the picture of a single, inhomogeneously broadened band of (C708) chls in *Synechocystis* PS I [33], although this band could result from two separate chl*a* dimers. We note that monomers of *Synechocystis* exhibit about 30% less red chls as compared to trimers [38,40].

Two separate red absorption bands are found in the 4 K absorption spectrum of the trimeric core particles of the cyanobacterium *S. elongatus* (Fig. 2, spectrum 2) with maxima at 708 nm (C708, corresponding to 4–6 chl*a*s) and 719 nm (C719, corresponding to 4 chl*a*s) [35]. The monomers show a 50% reduction of C719 [41] (not shown). In trimeric PS I cores of the cyanobacterium *Sp. platensis* (Fig. 2, spectrum 4) two red bands are found peaking at ~708 nm (C708, corresponding to approx. ~7 chl*a*) and 740 nm (C740, corresponding to ~3 chl*a*), the latter constituting the redmost absorbing species reported in any PS I complex. This very red shifted form is absent in monomeric complexes [42], although 1–3 C719 chls seem to be present [38]

(Fig. 2, spectrum 3). Careful comparison of the *Spirulina* monomeric and trimeric PS I spectra in Fig. 2 suggests that the increase of the C740 band is accompanied by the disappearance of an absorption band which peaks above 712 nm, suggesting that the C719 pool present in monomers may be further red shifted to 740 nm upon trimerization. Thus, all these PS I core particles share the presence of a C708 pool, while additional red forms are variable, both in amount and in spectral properties.

The presence of the low energy chls has a strong effect on the (steady-state) emission properties of the PS I core complexes. In *Synechocystis* core complexes, containing only 3–5 C708 red chlorophylls, the room temperature fluorescence emission spectrum exhibits a peak around 685–690 nm (F685) with a broad shoulder due to red chls at ~710 nm [30]. In contrast, in *Synechococcus* and *Spirulina*, which contain more and longer wavelength absorbing red chls, the room temperature emission peaks above 700 nm, with F685 only appearing as a shoulder [43,44].

At low temperatures the emission from the red pigments fully dominates all fluorescence spectra, which peak at ~720 nm in *Synechocystis* (F720) and ~730 nm in *Synechococcus* (F730) (trimers). In trimers of *Spirulina* at low temperatures one emission band is always present, peaking at ~730 nm (F730). A second emission band, with a maximum at ~760 nm (F760), may or may not be observed, depending on the oxidation state of P700: if P700 is preoxidized (using ferricyanide) F760 is absent, whereas it is present if the primary electron donor is reduced. The relatively strong spectral overlap of the F760 fluorescence with the absorption spectrum of $P700^+$ is thought to be the cause of this remarkable quenching of F760 emission [45]. Monomeric PS I cores of *Spirulina*, which do not exhibit the extreme C740 long wavelength chls, only show F730 fluorescence.

At room temperature the quantum yield of fluorescence of all PS I core particles is low [25], and the quantum yield of charge separation is more than 95%. A decrease of the temperature, however, induces a dramatic increase of the fluorescence quantum yield of these PS I particles [33,41,46], since a large fraction of excitations is trapped at the low energy chls at low temperatures. This is elegantly demonstrated in a long wavelength fluorescence excitation spectrum measured for PS I of *Synechococcus* at low temperature (Fig. 3). Excitation of the bulk antenna yields about 50% of the fluorescence as compared to direct excitation of the red chls, indicating that only about half of the excitations in this species are quenched in the RC without passing through the red chls. We note the clear 'dips' in the excitation spectrum at 686 and 698 nm, which in our view correspond to RC absorption bands of the primary electron acceptor A_0 and P700, which, upon excitation, have a very low probability of transferring energy to the emitting red chls.

3.1.2. Red chls in plant PS I complexes

In plants, the PS I complex PS I-200 can be separated into the PS I core and the peripheral light harvesting complex LHCI [11]. Each of these constit-

Table 1
6 K and room temperature low energy chl*a* absorption and emission

Species	Pool No. 1					Pool No. 2				
	absorption (nm)		emission (nm)		Number of chls/100	absorption (nm)		emission (nm)		Number of chls/100
	6 K	RT	6 K	RT		6 K	RT	6 K	RT	
Synechocystis monomers	708	703	720	712	~3	–	–	–	–	–
Synechocystis trimers	708	702	720	711	~5	–	–	–	–	–
Synechococcus trimers	708	702		707	~5	719	708	730	723	~4
Spirulina monomers	708	702[a]		712	5–7[a]	719	708[a]	730	721	~3[a]
Spirulina trimers	708	703		714	~7	740	715	760	730	~3
Maize PS I core	705		720		3	–	–	–	–	–
Maize LHCI	693		702		5	711		730		5

[a]These values represent another stoichiometry of red chls than estimated from the 6 K absorption spectrum.

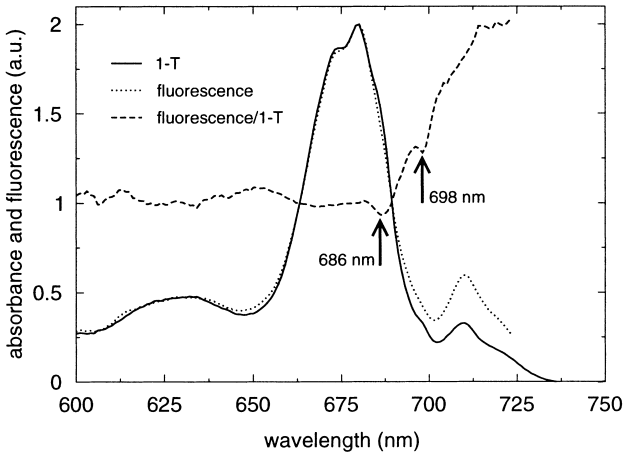

Fig. 3. 6 K fluorescence excitation spectrum of trimeric PS I core complexes of *S. elongatus*, detected above 780 nm (dotted), the 1-T spectrum (solid) and their ratio (dashed). The indicated 'dips' in our view represent the RC chls P700 and A_0.

uents contains a specific set of long wavelength chls. The PS I core of maize (Fig. 2, spectrum 5) mostly resembles the core of *Synechocystis*: at 4 K it exhibits one absorption band of red chls peaking around 705 nm (C705, ~3 chl*a*) (B. Gobets and J.A. Ihalainen, unpublished data) and has a low temperature emission maximum around ~720 nm (C720) [11]. LHCI (Fig. 2, spectrum 6) appears as a mixture of the LHCI-730 dimer and homo/heterodimers of Lhca2 and Lhca3 (see above). Recent experimental results indicate that a red chl pool with an absorption maximum at 711 nm is responsible for the low temperature emission of LHCI-730 [12]. Furthermore, recent fluorescence excitation and emission experiments on a mixture of Lhca1–4 have revealed another, new, low temperature emission band at 702 nm, corresponding to a pool of (relatively) red chls absorbing around 693 nm. These new spectral features may be the fingerprint of another dimer in LHCI [12]. Room temperature time resolved fluorescence measurements on the same preparation also indicate the presence of (at least) two spectroscopically different dimers in LHCI [47].

In PS I-200 the spectroscopic characteristics of the plant PS I core and LHCI are combined, resulting in a broad, featureless band of red chl absorption (Fig. 2, spectrum 7). At low temperatures the fluorescence of PS I-200 is dominated by emission from LHCI-730, resulting in the emission maximum at 730–735 nm that is characteristic of plant PS I [10].

3.2. The nature of the long wavelength chls

Energy selective fluorescence emission experiments at low temperature (6 K) have been performed to determine the homogeneous and inhomogeneous line widths of the bands of red chl, and to obtain their homogeneous line shape [33,35,48]. In all cases it was found that the Stokes' shift of the red chls is remarkably large. To illustrate this, in Fig. 4, energy selective emission spectra are presented for monomeric PS I cores of *Synechocystis*, which contain 3–4 C708 chls. The spectra are plotted on an energy scale, and are shifted relative to the wavelength of excitation, which is marked by a sharp scattering peak. For increasingly red shifted excitation wavelengths, the emission band converges to the homogeneous line shape, which exhibits a broad phonon wing. This phonon wing shows a maximum at 150 cm^{-1}, corresponding to a Stokes' shift of about 300 cm^{-1} (15 nm). Superimposed on the smooth phonon wing, a distinct progression can be discerned, at 25 cm^{-1} intervals. Both the large Stokes' shift and this progression are unique for the red pigments in PS I and are not observed in other chl*a* containing photosynthetic systems, such as LHCII, cytochrome b_6f and the PS II RC [49–51].

Preliminary modelling of the emission spectra in

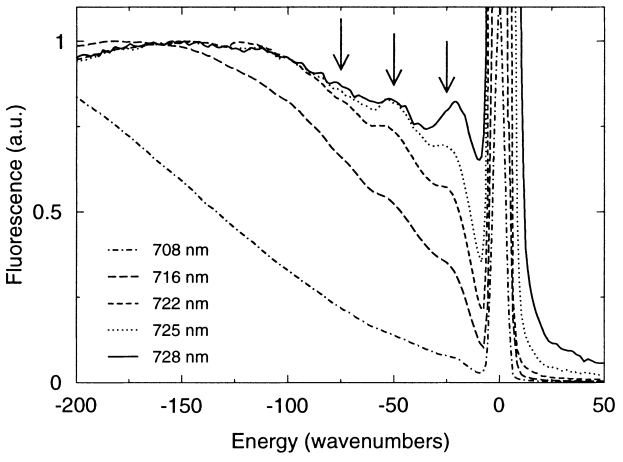

Fig. 4. 6 K energy selective emission spectra of monomeric PS I core complexes of *Synechocystis* PCC 6803 for increasingly red shifted excitation wavelengths. The spectra were shifted such that the scatter of the excitation light coincides with zero. The arrows at 25 cm^{-1} intervals indicate the phonon progression (see text).

Fig. 4 indicates that the Huang Rhys factor *S* for the phonons equals 3 or even more [48]. In a recent hole burning study by Rätsep et al. [40] on *Synechocystis* PS I this *S*-value was estimated to be 2. This should be compared to for instance LHCII for which an *S*-value of 0.6 was found [49]. The most straightforward interpretation of this remarkable difference is that the emitting species in *Synechocystis* is not a monomeric chl*a*, but for example (a) strongly coupled chl*a* dimer(s) or maybe even a larger aggregate of chl*a* [33]. For PS I complexes from *Synechococcus* and *Spirulina*, which exhibit even more red shifted chl pools, we find that these *S*-values are even larger and consequently we propose that also in these systems the red chls correspond to dimers or larger aggregates of chl*a*, in view of the further red shift and the larger number of chls involved in these red bands.

3.3. The function of the long wavelength chls

The function of the red chl species is still a topic of much debate. Intuitively it would appear that the effect of their presence would be a decrease in the overall efficiency of energy transfer to the reaction centre by forming local traps for excitations. Some authors have suggested, however, that in a non-equilibrium situation they may help increasing the efficiency of the system by concentrating excitations close to P700 [52–54,23,43]. Others argue that the red chls may have a role in photoprotection [52,37]. The above mentioned quenching of excitations located on the redmost pools of chls by $P700^+$ [45,37] could provide a pathway to prevent the formation of chl triplet states, which can lead to the formation of harmful singlet oxygen, under strong illumination conditions.

Another function of the low energy chls that has been proposed could simply be the increase of the cross-section for absorption of red light by the PS I antenna [55,56]. In a recent publication Rivadossi et al. investigated the importance of the long wavelength chls of PS I in photosynthetic light harvesting by leaves. It was demonstrated that although the PS I red forms account for only a few percent of the total light absorption in a normal 'daylight' environment, in a different 'shadelight' environment, depleted in $\sim$680 nm light, the long wavelength pigments may be responsible for up to 40% of total photon capture [57].

Alternatively, the red chls may simply be a consequence of the relatively dense packing of chls in the PS I core antenna: the chlorophyll concentration in the PS I core is significantly larger than in other photosynthetic antenna complexes. If chl is dissolved in an organic solvent at such a high concentration, such a solution exhibits some extraordinary properties: the fluorescence quantum yield decreases dramatically, whereas the absorption spectrum remains unchanged compared to lower concentrations [58]. This is thought to be the result of extensive energy transfer in the concentrated chl solution followed by quenching due to for instance a few unfavourably organized (sandwiched) chl*a* dimers. Such sites are apparently not present in PS I, since they would dramatically decrease the efficiency of the system. As a side effect the constraint of avoiding sandwiched pairs could result in the occurrence of some excitonically coupled head-to-tail dimers or larger head-to-tail aggregates with a strongly red shifted absorption maximum. A striking example of a system in which dense head-to-tail packing of pigments results in strong excitonic coupling are chlorosomes, the antenna complexes of green sulphur bacteria, which contain several thousands of Bchl*c* molecules. These antennae have a maximal absorption at 740 nm whereas monomeric Bchl*c* has an absorption maximum at 660 nm. In addition it was shown that the effective oscillator strength of Bchl*c* in chlorosomes was 7–8 times that of monomeric chls [59].

4. Dynamic experiments

4.1. Experimental considerations

The core antenna of PS I is intimately bound to the PS I reaction centre and unlike in antenna–RC complexes of photosystem II and bacterial photosystems it is not possible to biochemically separate the core antenna from the reaction centre. Therefore time resolved experiments on native PS I have to be performed on systems with a large number ($\sim$100) of chl*a* molecules which are all connected by energy transfer. Time resolved spectroscopic experiments on such large antenna–RC complexes re-

quire the use of very low energy excitation pulses, to avoid the process of singlet–singlet annihilation (see for a review [60,61]). This process can occur in complexes in which simultaneously two or more excitations are present: due to efficient energy transfer two excitations may collide at one single chl, which will then be raised to its second singlet excited state (S_2), from which rapid (<100 fs) internal conversion to the first singlet excited state (S_1) occurs. Singlet–singlet annihilation thus effectively removes excitations from the system resulting in additional non-physiological decay components. It must be stressed that in order to prevent singlet–singlet annihilation from occurring it is by far not sufficient to match the number of absorbed photons to the number of complexes in the sample volume. Since the distribution of absorbed photons is governed by Poisson statistics it can easily be shown that the fraction of excited complexes with more than one excitation is given by $P(>1)/P(>0) = (e^{\mu}-1-\mu)/(e^{\mu}-1)$ in which μ is the average number of excitations per complex. For $\mu = 1$ this yields 41% multiple excitations. In order to get this fraction below 10% each laser shot should excite less than one out of every four complexes, or to put it differently: only one out of 400 chls should be excited by each pulse. In practice this implies that pulse energies of a nJ or less have to be used. With such low energies a high repetition rate laser is required to limit the data acquisition time. Yet the repetition rate in its turn is limited by the requirement that before each new laser pulse the sample has to be either completely recovered from the previous excitation event, or has to be replaced by 'fresh' sample. Reduction of $P700^+$ in the presence of sodium ascorbate and PMS takes about 2 ms [46], thus limiting the repetition rate to ~ 500 Hz in case no sample refreshment is performed. This is almost always the case in low temperature experiments, since (rapid) sample refreshment in a cryostat is practically impossible. On the other hand, at room temperature the sample can be refreshed using a spinning cell or a flow cell with a (peristaltic) pump. With the former a repetition rate of about 100 kHz can be used safely, for a flow cell the repetition rate can generally not exceed 10 kHz, if total sample refreshment is required.

Even if experiments are performed very carefully, the detail of the processes that can be distinguished is limited. In an antenna–RC complex containing 100 chl molecules, in principle 100 separate lifetimes are present in the excitation decay process. One can at best resolve a fraction of those lifetimes, but only if relatively selective excitation and detection is possible. Since the individual absorption and emission spectra of the 100 chls in PS I cores are strongly overlapping, this condition of selectivity can only be met to a very limited extent, and consequently only a small number of (average) kinetic processes can be discerned.

4.2. Spectral-temporal processes in PS I

During the past decade, PS I complexes of a wide variety of species have been studied by several groups using (sub)picosecond time resolved spectroscopic techniques including pump probe [62,43,34,63–68], single photon counting (SPC) [43,32,4,69,46], fluorescence upconversion [70,71] and the use of a synchroscan streak camera [48,72,38]. The values of the time constants which have been found for aselective or bulk excitation at room temperature and which have been ascribed to various steps in the energy transfer and trapping processes in PS I are summarized in Table 2. We will illustrate the different processes that occur using Fig. 5, in which streak camera fluorescence emission data are shown for *Spirulina* trimeric PS I, along with the results of a global analysis fitting procedure [38]. In Fig. 5A,B, traces are shown for bulk (684 nm) and red chl (745 nm) emission, and the different lifetime components that contribute to the emission. Fig. 5C displays the decay associated spectra that resulted from a global analysis of these data.

The individual energy transfer steps between two chls are the fastest energy transfer events that occur in PS I. Since the excited state energy levels of these two chls are not necessarily different, it may not be possible to resolve these steps in isotropic measurements. Anisotropic pump probe or fluorescence upconversion techniques can reveal energy transfer between such isoenergetic pigments, provided that the absorption and emission dipole moments of donor and acceptor are not parallel. The lifetimes of these single step transfer processes in the PS I core antenna range between 100 and 200 fs [70,71]. The streak camera measurements displayed in Fig. 5 do not re-

veal these ultrafast processes. The fastest process recorded in these measurements (circles), which is fitted with a 0.4 ps time constant, does not reflect energy transfer, but represents the ingrowth of Q_y fluorescence upon relaxation from the initially excited Soret band [38]. (We note that the instrument response of 3 ps limited the accuracy with which this lifetime could be determined.)

Energy redistribution processes, during which the initial distribution of excited antenna molecules transforms into a thermally more equilibrated distribution, take place on a (somewhat) slower timescale. Since such equilibration processes involve energy transfer between chls absorbing at different energies, they appear as a decrease of fluorescence or bleaching in one part of the spectrum, and an increase of fluorescence or bleaching in another. In Fig. 5A–C the 3.9 ps (squares) and 15.0 ps (diamonds) components represent such spectral equilibration components. It must be stressed that equilibration lifetimes generally do not correspond to single step energy transfer processes, but reflect the overall result of a (large) number of those steps. Often equilibration components are not 'pure' in the sense that they also account for some non-equilibrium trapping, resulting in non-conservative energy transfer spectra, since the total decay exceeds the ingrowth. The 15.0 ps equilibration spectrum in Fig. 5C, which is only slightly negative above 740 nm, represents a clear example of such a non-conservative spectrum.

In order to accurately record the equilibration processes in PS I, high time resolution spectrally resolved techniques are required such as multicolour pump probe, fluorescence upconversion or the use of a synchroscan streak camera.

Spectral equilibration between the bulk chls, absorbing between 660 nm and 690 nm, occurs in about 500 fs [65,64,71] which, in view of the time constant for a single hop (100–200 fs), implies that only a few (< 5) hops are required to complete spectral equilibration among bulk chl*a*s in PS I. The lifetimes of the equilibration components between the bulk antenna and the various pools of red chls are species dependent and vary between 2 and 15 ps. For *Synechocystis* PS I, which we propose to exhibit only one single pool of red chls, usually only one single bulk

Table 2
Observed rate constants for different PS I complexes after aselective excitation at physiological temperature

Species	Single step transfer (fs)	Equilibration in bulk	Equilibration with red (ps)	Trapping (ps)	Ref.	Technique[a]
Chlamydomonas reinhardtii PS I core	180	5.4 ps			[70]	UPC
Synechocystis monomeric and trimeric PS I core			4.4–4.7	23–24	[38]	SSC
		500 fs	2.3	25	[65]	PP
		400 fs	4.8 or 2 and 6.5	22–24	[64]	PP
			3.7	24	[34]	PP
			5	24–25	[4]	SPC
Synechococcus trimeric core	130	360 fs	3.6 and 9.6	38	[71]	UPC/SSC
			3.8 and 9.6	36	[38]	SSC
			7–12	30–35	[43]	SPC/PP
			14	38	[46]	SPC
Spirulina monomeric core			3.7 and 12.9	38	[38]	SSC
			9	28, 69	[69]	SPC
Spirulina trimeric core			4.3 and 15.1	51	[38]	SSC
			9	31 and 65	[69]	SPC
Plant core			8.0	22	B. Gobets, J.A. Ihalainen, unpublished data	SSC
PS I-200			5.4 and 15	67	B. Gobets, J.A. Ihalainen, unpublished data	SSC
			11	57 and 130	[97]	SPC

[a]UPC, fluorescence upconversion; SSC, synchroscan streak camera; PP, pump probe; SPC, single photon counting.

to red equilibration component is reported, with a lifetime of 4–5 ps [4,34,38,48,64,66]. However, recently equilibration lifetimes of about 2 ps were reported [64,65]. Savikhin et al. even report a second equilibration component with a lifetime of 6.5 ps. Such biexponential equilibration between bulk and red chls seems to be consistent with the two distinct red pools that have been proposed by Hayes et al. [39] (see above), but contradicts with other time resolved spectroscopy results. This apparent discrepancy so far remains unsolved.

In *Synechococcus* PS I cores, which exhibit two distinct pools of red chls, clearly two distinctly different equilibration components are observed, with lifetimes of 3.8 and 9.6 ps [38]. These two separate lifetimes could not be resolved in earlier SPC experiments, which have yielded only a single lifetime of 12–14 ps [43,46]. We note that this single lifetime and its associated spectrum have been the inspiration for a series of serious modelling attempts [24,43,46,73].

Like *Synechococcus* PS I, both *Spirulina* monomeric and trimeric PS I particles also exhibit two distinct bands of red chls, and consequently also in these systems equilibration with the red chls is biexponential [38]. In *Spirulina* monomeric PS I, fast equilibration between the bulk and the red chls occurs in 3.4 ps, and slower equilibration, including a considerable amount of non-equilibrium trapping, occurs in 11.6 ps. In the trimeric PS I particles from *Spirulina*, the lifetimes of both equilibration components are somewhat slower, 3.9 ps and 15 ps respectively (Fig. 5). Also for these complexes the SPC technique has failed to accurately disentangle these two equilibration processes.

The excitation dynamics in the PS I core of plants seems to be quite similar to that of *Synechocystis*: since it contains only one pool of red chls, it exhibits only one single equilibration component with these red chls, with a lifetime of 8 ps, which is somewhat slower than observed in *Synechocystis* PS I (B. Gobets and J.A. Ihalainen, unpublished data). In PS I-200 a 5.4 ps equilibration lifetime is observed, which we assign to equilibration processes taking place both in the core and in LHCI. A second, 15 ps component probably represents a mixture of equilibration between the core and LHCI, equilibration within LHCI, and trapping from the core (B. Gobets and J.A. Ihalainen, unpublished data).

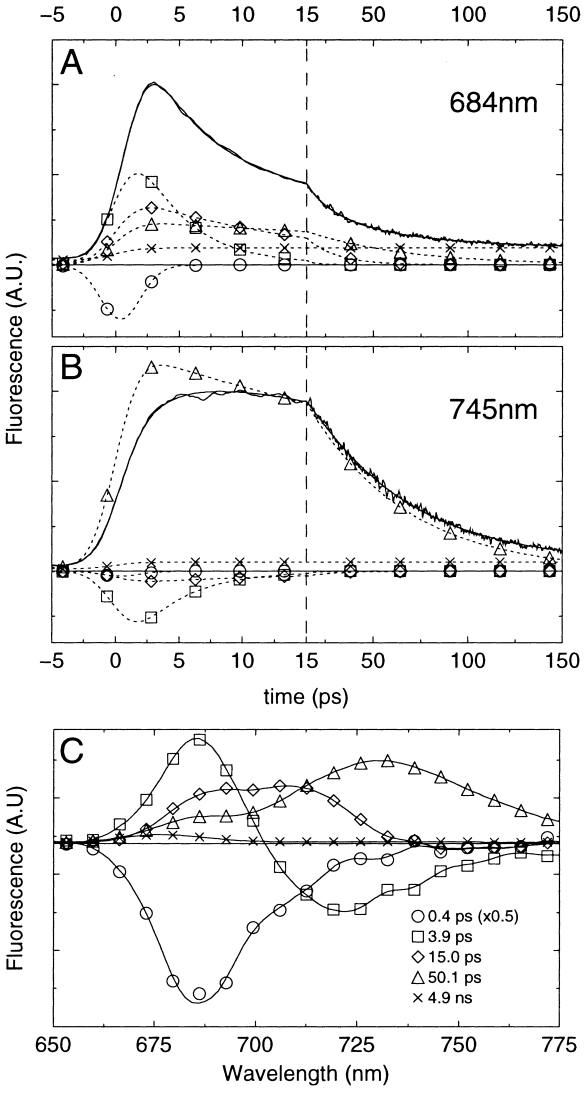

Fig. 5. Room temperature time resolved emission of trimeric PS I particles of *Sp. platensis* for excitation at 400 nm. (A) Bulk emission trace taken at 684 nm (noisy solid), the global analysis fit (solid) and the various lifetime contributions (dashed with markers). Notice the trace is plotted on a linear-logarithmic scale. (B) As A, but for detection of red chl emission at 745 nm. (C) Decay associated spectra resulting from the global analysis fit. The fitted lifetimes were: 0.4 ps (○), 3.9 ps (□), 15.0 ps (◇), 50.1 ps (△) and 4.9 ns (×).

The general trend in all these complexes is that the rate of equilibration between the bulk chls and a pool of red chls increases with the size of the red pool, and the excited state energy of the chls con-

tained in it, which is qualitatively consistent with the concept that these times reflect on one hand the search time in the PS I antenna and on the other hand the spectral overlap factor between the bulk and red chls.

The slowest process observed in all PS I cores is the trapping kinetics, representing the overall rate at which excitations disappear from the system by charge separation in the RC, after all spectral evolution processes have been completed. In time resolved fluorescence spectroscopy experiments, trapping appears as the slowest component of the system, showing a fluorescence decay at all wavelengths of detection. In pump probe experiments trapping is observed as the rate at which the spectrum of $P700^+$ is formed (which generally lives infinitely on the timescale of these experiments). Since the trapping component typically has a lifetime of (several) tens of ps, it can be recorded quite accurately even with relatively low time resolution techniques such as SPC. In Fig. 5 trapping is reflected by the 50.1 ps process (triangles), which exhibits an all positive spectrum (Fig. 5C). The relative ease of recording the trapping kinetics is reflected by the consistency of the values, both for the trapping times in PS I cores from *Synechocystis* (22–25 ps) and *Synechococcus* (30–38 ps) using a variety of techniques. In *Spirulina* PS I core monomers, which has a red chl composition quite similar to that of *Synechococcus* trimeric PS I cores, trapping occurs in 38 ps, while in the trimeric PS I cores from *Spirulina*, which exhibit the extreme C740 red chls, the observed trapping time is 50 ps (Fig. 5) [38]. Trapping in the plant core is similar to that of *Synechocystis*, and occurs in 22 ps, in agreement with the similar spectral properties of both cores.

These results clearly demonstrate the trend that a larger number and lower energies of red chls result in a slower trapping component. Whereas red chl contents and spectral properties constitute the key difference between the various core complexes, PS I-200 is a structurally different system due to the presence of the peripheral LHCI complexes. Therefore the observed relatively slow 67–130 ps trapping time is not only the result of the large number of red chls, but also reflects the much larger average distance between the antenna chls in LHCI and the RC.

The very slow 4.9 ns process (crosses) in the fit displayed in Fig. 5 represents a contribution by some free chls in the preparation and therefore does not reflect a process in the PS I core.

5. Quantitative (target) analysis

So far we have made some qualitative remarks about the relation between the observed lifetimes in the various PS I core complexes and the amounts and energies of the red chls present. Also the energies of the red pools, and their respective emission spectra, have only been characterized at non-physiological, low temperatures. In order to make more quantitative statements about the effects of the red chls upon the energy transfer and trapping in PS I cores, and their absorption and emission properties under physiological conditions, we have recorded the fluorescence dynamics and spectral evolution of both monomeric and trimeric PS I core complexes from *Synechocystis* and *Spirulina*, and trimeric PS I core complexes of *Synechococcus* under identical experimental conditions at room temperature, and performed a target analysis of these data [38].

5.1. Model

We used the target analysis to test the hypothesis that the observed large kinetic differences between the different cyanobacterial core complexes can all be explained entirely in terms of the differences in the content and spectral properties of the red chls, implying that the properties of the bulk chl antenna do not differ significantly between these core complexes.

The time resolved fluorescence experiments were performed with a synchroscan streak camera with a spectrograph which has an instrumental response of $\sim$3 ps, allowing us to resolve kinetics occurring significantly faster than 1 ps [38]. Using other techniques, either time traces are measured sequential for different detection wavelengths, or spectra are measured sequential for different delay times. In contrast, the streak camera setup records spectral and temporal data simultaneously, resulting in time resolved fluorescence spectra of unprecedented quality allowing for a quantitative target analysis.

Here we will summarize the procedure and results

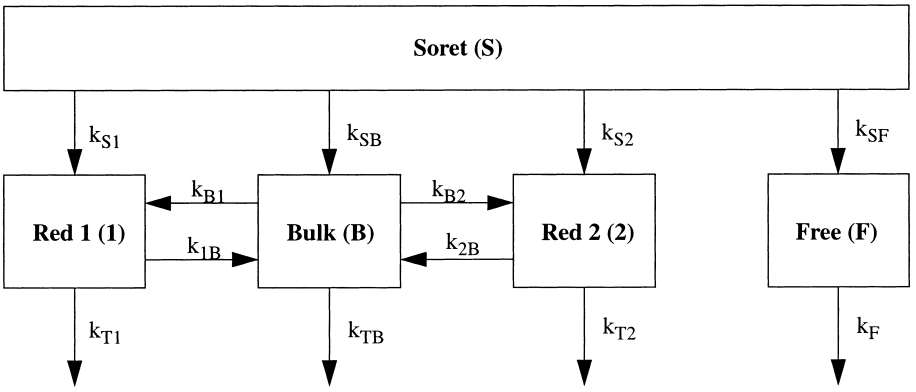

Fig. 6. Compartmental model describing the kinetics of different cyanobacterial PS I core particles upon excitation at 400 nm.

presented in [38]. The compartmental model used to analyse the time resolved fluorescence data is presented in Fig. 6 and consists of five compartments, representing the Soret state (S) of all spectral forms, and the Q_y states of the bulk chl pool (B), two red shifted chl pools (1 and 2) and a pool representing free chls which are not connected to the PS I core (F), but which have to be accounted for. The RC chls were not included in a separate compartment, since we aim to describe the energy transfer in the antenna rather than the intricate details of charge separation in the RC. Moreover, the number of RC pigments is small, and their spectral properties differ relatively little from those of the bulk chls. Therefore the (fast) kinetics of charge separation are not revealed directly by our data. For the modelling of *Synechocystis* PS I, one of the pools of red shifted chls was omitted from the scheme.

The following rate constants were included in the model. (1) From the Soret compartment irreversible energy transfer occurs to the three or four Q_y compartments with the rate constants k_{SB}, k_{S1}, k_{S2} and k_{SF}. The sum of these rate constants, which represents the observed Soret–Q_y relaxation rate, measured 1.2–2.5 ps^{-1}. The four individual rates do not have an actual physical meaning, they merely account for the initial distribution of the excitations over the different compartments, and were adjusted such that all chls had an equal probability to be excited (aselective excitation). (2) Uphill and downhill energy transfer occurs between the red chl compartments and the bulk chl compartment with rate constants k_{B1}, k_{B2}, k_{1B} and k_{2B}.

We have not included direct energy transfer between different pools of red chls since low temperature fluorescence emission spectra of *Spirulina* trimeric PS I indicate that energy transfer between different pools of red chls is not very efficient [42], although energy transfer may occur between the two red pools in *Synechococcus* trimeric PS I [35]. At this point we discard it as a secondary effect. (3) Trapping occurs from the bulk chls and the red chl compartments with rate constants k_{TB}, k_{T1} and k_{T2}. It was found that all data sets could be described well using a fixed value of k_{TB} of $(18\ ps)^{-1}$, in accordance with our hypothesis that the properties of the bulk antenna are very similar for all PS I core complexes. (4) Free chl emission decays with a rate constant k_F, which measured about 0.2 ns^{-1}. Since discrete spectral pools are used, inhomogeneous broadening, although known to be large for the long wavelength chls [33,35], is not explicitly included in our model. The model described above was used to analyse our data, and we will discuss some specific results. More details of this analysis are reported in [38].

Various kinetic models have been proposed [32,43,64,74–76] to model time resolved fluorescence or transient absorption measurements of PS I. In most of these models a 'funnel'-like configuration of the various spectral types was proposed [32,43,64,75,76], in which the bulk antenna chls transfer energy to the red chls, which subsequently transfer energy to P700. Holzwarth et al. [43] and Savikhin et al. [64] also proposed a model in which trapping occurred exclusively from the bulk chls.

All these models explicitly assume the red chl forms to be located either very close to, or very distant from P700. Only Searle et al. [74] proposed a

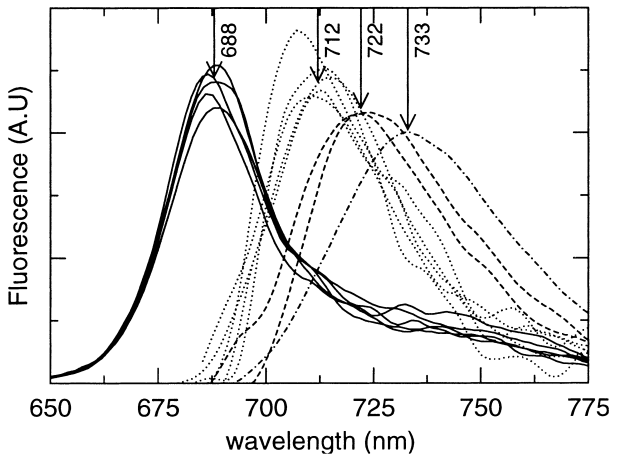

Fig. 7. Species associated emission spectra of target analysis of fluorescence decay of different cyanobacterial PS I core particles upon excitation at 400 nm. Arrows indicate the approximate maximum of the bulk spectra (black), C708 spectra (dotted), C719 spectra (dashed) and C740 spectrum (dot-dashed).

model, similar to our model presented in Fig. 6, which allowed for trapping both from the bulk chls and the red chls. We note, however, that only Turconi et al. [32] and Holzwarth et al. [43] actually used their models to perform a target analysis of their data.

5.2. Species associated emission spectra

The species associated emission spectra (SAES) of the different pools of chls, resulting from the target analysis of the five different PS I preparations, are presented in Fig. 7. All spectra are simply plotted together to demonstrate the striking similarities between the results obtained for different PS I particles. In all species the emission from the bulk compartment is represented by a spectrum (solid), which exhibits a maximum around 688 nm and which shows a distinct long red tail, extending beyond the window of observation. Except for a 12 nm red shift, the spectra are nearly indistinguishable from the emission spectrum corresponding to the free chl compartment (not shown), which in its turn is very characteristic for the emission of monomeric chl*a* in solution [28]. The fact that the bulk spectra are indistinguishable between the different PS I species underlines the absence of clear differences in the dominating band of the absorption spectra between different PS I core particles.

Also the spectra corresponding to the first (C708) pool of red chls (dotted), present in all studied cyanobacterial PS I core complexes, appear quite similar for all studied species, underpinning the strong similarity between C708 chls contained in the PS I cores of the different species. The C708 spectra are considerably broader than those of the bulk chls, reflecting the strong homogeneous and inhomogeneous broadening in this red chl pool [33,35,40]. Note that the maxima of these spectra all appear around 712 nm, at significantly higher energy as compared to the low temperature emission.

Probably even more remarkable are the emission spectra corresponding to the C719 pool (dashed), which represents the second pool of red chls occurring in *Synechococcus* PS I trimers and *Spirulina* PS I monomers, and which are practically identical. The maxima of these spectra occur at about 722 nm, and their width is somewhat larger than for the first (C708) pool of red chls, reflecting the even larger (in)homogeneous broadening of these pools [35]. The emission spectrum of the C740 pool (dot-dashed), which is the second pool of red chls in *Spirulina* trimers, reaches a maximum at 733 nm, and the spectrum is again broader than that for the C719 pool, reflecting an even larger (in)homogeneous broadening of this pool.

The maxima of all the room temperature emission spectra of the different pools of red chls occur at wavelengths that are considerably blue shifted with respect to their low temperature emission spectra. Part of this may be due to emission from higher energy red chls within the inhomogeneous distribution, which are not populated at low temperatures. Another part may be explained by a significant blue shift of the absorption maxima of these red pools at room temperature [40] (see also below).

5.3. Energies of red chls at room temperature

The forward and backward energy transfer rates [38] between the red and the bulk chls pools resulting from the target analysis, together with the stoichiometric estimates listed in Table 1, were used to calculate the energy difference between the red chl pools and the bulk chls. To do so we applied the concept of detailed balance, stating that the energy difference between two different pools of chls, A and B, can be

expressed as $\Delta E = k_b T \ln(N_A k_{AB}/N_B k_{BA})$, in which k_b represents Boltzmann's constant (0.695 cm^{-1} K^{-1}), T the absolute temperature, N_x the number of chls in pool x, and k_{xy} the transfer rate from pool x to pool y. Doing so, we find for the C708 pool in all studied PS I particles a value of ΔE which varies between 350 and 515 cm^{-1}, corresponding to a room temperature absorption maximum of this pool at around 702 nm, which is consistent with the 702–704 nm value reported by Rätsep et al. [40], and also seems reasonable in view of the ~712 nm emission maximum of this pool (see above), and the 10 nm Stokes' shift we reported previously [33].

Applying the stoichiometry listed in Table 1, the energy difference of the second (C719) pool of red chls in *Synechococcus* trimeric and *Spirulina* monomeric PS I is found to be approx. 570 cm^{-1}, corresponding to an absorption maximum of ~708 nm. This value seems to be realistic in view of the emission maximum of this pool which appears around 722 nm. The 11 nm blue shift of the absorption maximum of the C719 pool from 719 nm to 708 nm upon increasing the temperature from 6 K to room temperature is considerably larger than the 4–6 nm shift found for the C708 pool ([40]; see above), which indicates that the chls in the C719 pool are more strongly coupled to their environment than those in the C708 pool.

The energy difference between the second red pool in *Spirulina* trimeric PS I (C740) and the bulk is about 725 cm^{-1}, which corresponds to an absorption maximum at 715 nm. Also this value we consider realistic in view of the emission maximum at 733 nm. The apparent Stokes' shift of 18 nm is comparable to the 20 nm Stokes' shift found at 6 K. The blue shift of 25 nm upon a rise of the temperature from 6 K to room temperature is about 5 times more than found for the C708 chls ([40]; see above) and about 2 times more than found for the C719 chls (see above), indicating an even stronger coupling of the chls in this extremely red shifted pool to their local environment.

In all cases we observe that the energy of the red chls is considerably higher at room temperature as compared to low temperatures. This could be caused by the breakdown of the coherence length in the chl aggregates responsible for the red chl forms, due to dynamic disorder at higher temperatures. A second mechanism responsible for the temperature dependence of the red shift could be a (local) contraction of the protein at low temperatures, causing a change of the distances between the chls. A similar mechanism was proposed to account for the temperature dependent shift of the energy of the special pair in the bacterial photosynthetic reaction centre [77].

5.4. Trapping

If the bulk trapping rate, k_{TB}, is regarded as a free parameter of the fit, its value varies between (17 ps)$^{-1}$ and (29 ps)$^{-1}$ in the different PS I cores. Despite this spread of values, it turns out that the quality of the fit decreases only slightly by fixing this value to (18 ps)$^{-1}$. Earlier modelling of the dynamics in *Synechocystis* and *Synechococcus* PS I, based on the chl coordinates from the structure of *Synechococcus* PS I [72], also resulted in an 18 ps trapping time upon removal of two putative red chls, which strongly suggests that this is indeed the trapping time in a bulk PS I without red chls.

The trapping rates from any pool of antenna chls depend in first order on the weighed (average) distance of these chls to P700, their relative orientation to P700, and the overlap integral of their emission spectrum with the absorption of P700. If the average location and orientation of the chls in a red pool are not very different from the bulk chls, the relative trapping rate from that pool as compared to the bulk chls only depends upon the relative spectral overlap between the emission of these red chls with the absorption of P700 as compared to the bulk chls. At low temperatures this overlap is very small, resulting in slow trapping from the red chls, and a low quantum efficiency of charge separation. Upon an increase of temperature the overlap increases due to a number of causes. First of all the emission (and absorption) of the strongly coupled red chls blue shifts quite significantly, towards the absorption of P700 [40] (see also above). Secondly, in the pools of red chls, which are significantly inhomogeneously broadened, at low temperatures excitations mainly reside on the lower energy chls in the distribution, whereas at higher temperatures, also the higher energy chls in the distribution can be excited, which results in a further blue shift of the (average) emis-

sion of the red chls. Finally, the absorption band of P700 and the intrinsic emission of the individual red chls broaden with increasing temperature.

The relative overlap integrals of the various chl pools with P700 may be estimated from the emission spectra resulting from the target analyses, and a P700 absorption spectrum, which we approximate by a Gaussian with a full width at half of the maximum of 20 nm, peaking at 698 nm [41]. The overlap integrals of the pools of red chls with P700 that are calculated this way, turn out to be quite significant: overlap integrals of the C708, C719 and C740 pools with the P700 absorption spectrum are estimated to be about 80%, 30% and 15% of the overlap of the bulk emission with the P700 absorption spectrum, respectively. The accuracy of the smaller numbers is limited, since they depend strongly upon the exact properties of the extreme blue edge of the emission spectra obtained from the target analysis.

The relative overlap integrals thus estimated may be compared to the (relative) trapping rates which result from the target analysis. The trapping rates k_{T1} from the first pool of red chls (C708) are all of the same order as k_{TB}, and therefore roughly match the 80% relative overlap integral [38]. Monomeric PS I of *Synechocystis* is the only exception with a value of k_{T1} which is only about 10% of k_{TB}. Since these monomers contain approx. 30% less C708 chls as compared to trimeric PS I from the same species, possibly the preparation of monomeric particles is heterogeneous, in the sense that some particles may contain as many red chls as the trimers.

The trapping rates k_{T2} from the second pools of red chls measure only 10% of k_{TB} or less, which is lower than expected from the decrease in overlap integral indicated above. It must be noted that, in contrast to the trapping rates from the first pool of red chls, the quality of the fit does not depend too strongly upon these (slow) trapping rates, and therefore they merely represent an 'order of magnitude' estimate.

These results indicate that the C708 chls are probably located neither exceptionally close to the RC, nor at great distance. In other words, in our view C708 could be two dimers of chl*a*, located somewhere in the ring of bulk chls, not necessarily in some 'special' position. On the other hand, our results are still consistent with a more peripheral location of the more red shifted pools (C719 and C740), in accordance with biochemical data.

6. Structure based simulation

In the absence of a three-dimensional structure, modelling was until recently essentially limited to square or cubic lattice models (see for instance [24,78,21]). One of the key problems in these earlier simulations was the positioning of the trap, relative to the surrounding antenna. Moreover, the quality of the data at that point did not really allow for extensive quantitative analysis.

Since the recent publication of a 4 Å resolution three-dimensional structure of trimeric PS I core particles from the cyanobacterium *S. elongatus* by X-ray diffraction on crystals [7,8], more realistic modelling has become possible [46,48,64,72,80], although a full calculation of energy transfer in PS I based on this structure is still not straightforward. First of all, information about the orientation of the transition dipole moments of the chls is currently missing. Secondly, the positions of the different chl spectral forms are unknown. Finally, the structure is known only for *Synechococcus* PS I. In view of the spectroscopic differences, small variations of the protein structure and chl binding sites must be present between the different PS I species that we have investigated, although the global organization of different PS I species is expected to be conserved to a high degree. Even if these difficulties are overcome (by obtaining a high resolution structures of the relevant proteins), relating the structure of a photosynthetic protein to spectroscopic data has proven to be very difficult, even for systems with a much smaller amount of chls, such as for instance the FMO antenna complex [81,82] or LHCII [83].

Here we will show, however, that some general features of the kinetics in the PS I core system can be derived from a simulation based on the 4 Å structure. The results of the target analysis, which were presented above, can be used as an input for such a simulation: overlap integrals can be estimated from the room temperature absorption and emission properties of the different pools of (red) chls, and moreover the target analysis has learned us that the kinetics of a (hypothetical) PS I core particle without

low energy chls will exhibit a slowest decay component (trapping time) of approx. 18 ps. Here we will investigate the dynamics of such a PS I core particle, which has the great advantage that it relieves us from the problem of locating the red chls in the structure, such as in [46,48,64,72,79,80]. The resulting values of the fitting parameters can subsequently be used as a constraint for the simulation of 'real' PS I core particles, which do contain red chls.

The simulations were performed basically as described in [72]. We have assumed the Förster mechanism to be the dominant mechanism for the energy transfer in PS I. We calculated the 89×89 k-matrix of Förster transfer rates between each pair of chls i and j, k_{ij}, using the expression $k_{ij} = FA_{ij}r_{ij}^{-6}$, in which r_{ij}, the distance between chl i and j, was obtained from the structure. A_{ij} represents the overlap factor between the absorption spectrum of acceptor chl i and the emission spectrum of donor chl j. The overlap factors for downhill energy transfer were obtained from the shifted absorption and emission spectra of free chls, except for the absorption spectrum of P700 which was approximated by a Gaussian shaped absorption band peaking at 698 nm and a full width at half of the maximum of 19 nm. The reverse, uphill rates were calculated using the constraint of detailed balance (see above). The absorption maxima of the other RC chls were primary electron acceptor (A_0), 686 nm and accessory chls, 680 nm. For the antenna two spectral compositions were investigated: an isoenergetic antenna with an absorption at 680 nm, and a heterogeneous antenna which contained equal ratios of chls absorbing at 670, 680 and 690 nm, which were distributed randomly. The factor F is a scaling factor, that accounts for all other factors in the Förster formula (orientations, index of refraction) and which effectively determines the average single site lifetime, τ_{ss}, which is defined as the time needed for an excitation to hop away from a chl site, averaged over all possible sites. This scaling factor F and the intrinsic trapping time τ_{trap}, from the chls identified as P700, are the only two parameters of the simulation. The lifetimes in the system were obtained by calculating the eigenvalues of the k-matrix.

For both spectral compositions of the antenna, we have looked for combinations of the average single site lifetime τ_{ss} (which is determined by F) and τ_{trap} that result in a slowest time constant of 18 ps in the kinetics of the system. This results in the curves plotted in Fig. 8. It immediately strikes the eye that the relation between τ_{ss} and τ_{trap} is almost (but not perfectly) linear. Such a linear relationship was predicted by Pearlstein [84], Kudzmauskas et al. [85] and den Hollander et al. [86], but we note that such relations were derived for a regular (square) lattice of isoenergetic chromophores, and that it is thus not straightforward that such a linear relation also holds for a non-regular, three-dimensional lattice, such as the PS I core antenna, especially in the case of the (slightly) heterogeneous bulk antenna. Furthermore, the equation contains a so-called structure factor, which can be calculated for a regular lattice (see e.g. Somsen et al. [87]), but which is unknown for the PS I structure.

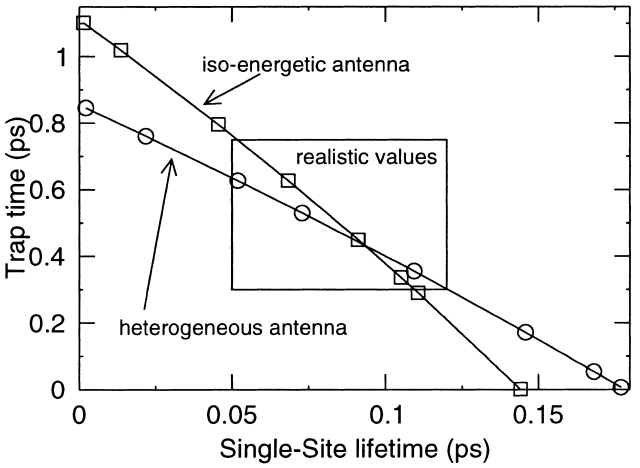

Fig. 8. Combinations of the intrinsic trap time and single site lifetime that result in an 18 ps observed trap time. The circles represent the curve for a heterogeneous antenna whereas the squares represent the homogeneous antenna (see text). The box encloses the region of the graph which in our view represents realistic values of the parameters.

The two lines in Fig. 8 provide upper limits for both τ_{ss} and τ_{trap}, of 200 fs and 1.2 ps, respectively. More realistically the value of τ_{trap} should not be less than $\sim$350 fs, and likewise the value of τ_{ss} should be more than 50 fs. This restricts the parameters to the values within the box drawn in Fig. 8. This limits τ_{ss} between 50 and 120 fs, which is somewhat faster than the measured fluorescence depolarization times of 130–180 fs [70,71], but since these measurements do not necessarily reflect the real single step transfer time, but are in fact expected to show a somewhat

longer time, the agreement between the simulation and the experiment can be considered rather good. The box in Fig. 8 limits the intrinsic trapping time, τ_{trap}, between 350 and 800 fs, which is significantly faster than the 1.4–3 ps values reported earlier [66,67,79], but consistent with more recent reports [48,68,73,80]. This is fast compared to for instance the purple bacterial RC, in which charge separation from the primary electron donor occurs in 3 ps [88], but comparable to the 400 fs charge separation as found by Groot et al. [89] in PS II. In PS II the coupling of the two chl*a*s constituting the primary electron donor P680 is less strong as compared to the bacterial primary electron donor, and comparable to the coupling with the other RC chls. Therefore a so-called multimer model was proposed for PS II [90], which may also be applicable for PS I [91].

Recently it was shown that multiple pathways of charge separation exist in the purple bacterial RC, i.e. electron transfer cannot only take place from P*, but also from B* [92–94]. Similar results were obtained for the RC complex of green sulphur bacteria, which resembles the RC of PS I [95,96]. Such pathways may prove to be a universal feature of photosynthetic RCs. However, whereas in purple bacteria and green sulphur bacteria the excited state energy levels of respectively B and chl*a* 670 are too high to be accessible from the antenna, all energy levels exciton manifold in a multimer PS I or PS II RC are more or less degenerate with the antenna, and therefore alternative pathways of electron transfer would all sum up to one fast effective rate of electron transfer, even for aselective excitation of the antenna.

In Fig. 1, we have indicated some typical transfer rates, which were derived from the simulation with a trapping time τ_{trap} of $\sim$500 fs. This is within the realistic regime, and the simulations with either a isoenergetic or a heterogeneous antenna both yield approximately the same values. The hopping between nearest neighbours in the antenna on the average takes 150–200 fs, a value that agrees with those found in fluorescence depolarization experiments [70,71]. Tens to hundred of these elementary steps are required to reach a specific site in the antenna, such as a cluster of red chlorophylls, which therefore takes about 2–15 ps, dependent on the exact location and spectral properties of such a cluster. The transfer rate from a bulk chl to a neighbouring red chl is only slightly lower (35–75%) as compared to the transfer between two neighbouring bulk chls, but the back transfer from the red chls is dramatically lower (1–8%).

The average time needed for an excitation to hop from a bulk chl directly to the RC amounts several tens of ps. However, the effective trapping time in a PS I core particle, lacking red chls, is as low as 18 ps. This implies that hopping to the RC does not occur directly from an average bulk antenna chl, but rather from a selection of chls that are relatively close to the RC.

The 'linker' chls, two antenna chls which are located relatively close to the RC (L1 and L2 in Fig. 1), have been proposed to play an important role in guiding excitations from the antenna to the RC [9]. Within our model we can investigate how important these two chls actually are for the energy transfer in PS I. First of all we can determine which fraction of excitations passes through the linker chls, by setting all reverse rates from the linker chls to zero, we can determine that the fraction of excitations which passes at least once through each of the linker chls is 60–70%. This seems to be a large fraction, but in fact this number is not unlike the values found for the other antenna chls, which is not surprising if one realizes that in the 18 ps before trapping, about 100–250 'hops' occur.

A more easy way of determining the importance of the linker chls is simply by leaving them out, and see how this affects the overall trapping time. Both for an isoenergetic and heterogeneous antenna, for realistic values of τ_{ss} and τ_{trap}, removal of the linker chls slows down trapping only by about 6%, and for more extreme cases up to 16%. This of course is negligible compared to the effect that the red chls have upon trapping, slowing it down by almost a factor of 3 in the case of *Spirulina.*

7. Concluding remarks

We have shown that the dynamics of different PS I preparations can be described by a single unifying model, consisting of a bulk compartment of which the properties are species independent and a number of compartments representing the red chls, the properties of which vary between different species. Con-

sequently the total dynamics are governed by both system dependent and system independent parameters. First of all the transfer from the bulk chls to the RC is mainly governed by the average distance between the antenna and the RC, since equilibration in the bulk antenna takes place on a sub-ps time scale. This parameter, together with the intrinsic rate of charge separation by P700, fully determines the dynamics of a PS I core system without red chls, and thus represents the system independent parameters contributing to the dynamics of any PS I core particle. The (large) kinetic differences between the various PS I particles arise from differences in the red chl content. Both the number of red chls and their excited state energies are found to be the basic system dependent parameters that determine the dynamic variety between different PS I core particles.

The fast hopping time in the antenna only affects the overall dynamics in an indirect way. The fast radial energy transfer towards the RC is not limiting the kinetics, but the tangential energy transfer around the ring eventually determines the fraction of excitations that reaches the low energy chls.

The presence of the two so-called linker chls does not have a significant effect upon the overall dynamics. As for the position of the low energy chls, the C708 pool is neither positioned very close to the RC, nor far away. The other C719 and C740 are probably located more peripherally, possibly in the trimerization domain.

References

[1] A. Cantrell, D.A. Bryant, Plant Mol. Biol. 9 (1987) 453–468.
[2] U. Mühlenhoff, W. Haehnel, H. Witt, R.G. Herrmann, Gene 127 (1993) 71–78.
[3] H.V. Scheller, H. Naver, B.L. Moller, Physiol. Plant. 100 (1997) 842–851.
[4] S. Turconi, J. Kruip, G. Schweitzer, M. Rögner, A.R. Holzwarth, Photosynth. Res. 49 (1996) 263–268.
[5] J. Kruip, D. Bald, E. Boekema, M. Rögner, Photosynth. Res. 40 (1994) 279–286.
[6] E.J. Boekema, P.E. Jensen, E. Schlodder, J.F.L. van Breemen, H. van Roon, H.V. Scheller, J.P. Dekker, Biochemistry 40 (2001) 1029–1036.
[7] P. Fromme, H.T. Witt, W.-D. Schubert, O. Klukas, W. Saenger, N. Krauss, Biochim. Biophys. Acta 1275 (1996) 76–83.
[8] N. Krauss, W.-D. Schubert, O. Klukas, P. Fromme, H.T. Witt, W. Saenger, Nat. Struct. Biol. 3 (1996) 965–973.
[9] W.-D. Schubert, O. Klukas, N. Krauss, W. Saenger, P. Fromme, H.T. Witt, J. Mol. Biol. 272 (1997) 741–769.
[10] S. Jansson, Biochim. Biophys. Acta 1184 (1994) 1–19.
[11] R. Croce, G. Zucchelli, F.M. Garlaschi, R.C. Jennings, Biochemistry 37 (1998) 17355–17360.
[12] J.A. Ihalainen, B. Gobets, K. Sznee, M. Brazzoli, R. Croce, R. Bassi, R. van Grondelle, J.E.I. Korppi-Tommola, J.P. Dekker, Biochemistry 39 (2000) 8625–8631.
[13] S. Jansson, B. Andersen, H.V. Scheller, Plant Physiol. 112 (1996) 409–420.
[14] V.H.R. Schmid, K.V. Cammarata, B.U. Bruns, G.W. Schmidt, Proc. Natl. Acad. Sci. USA 94 (1997) 7667–7672.
[15] R. Croce, R. Bassi, in: G. Garab (Ed.), Photosynthesis: Mechanisms and Effects, Vol. 1, Kluwer, Dordrecht, 1998, pp. 421–424.
[16] W. Kühlbrandt, D.N. Wang, Y. Fujiyoshi, Nature 367 (1994) 614–621.
[17] R. Simonetto, M. Crimi, D. Sandona, R. Croce, G. Cinque, J. Breton, R. Bassi, Biochemistry 38 (1999) 12974–12983.
[18] E.J. Boekema, R.M. Wynn, R. Malkin, Biochim. Biophys. Acta 1017 (1990) 49–56.
[19] O. Klukas, W.D. Schubert, P. Jordan, N. Krauss, P. Fromme, H.T. Witt, W. Saenger, J. Biol. Chem. 274 (1999) 7361–7367.
[20] Y. Deligiannakis, J. Hanley, A.W. Rutherford, Biochemistry 37 (1998) 3329–3336.
[21] T.G. Owens, S.P. Webb, L. Mets, R.S. Alberte, G.R. Fleming, Proc. Natl. Acad. Sci. USA 84 (1987) 1532–1536.
[22] M. Beauregard, I. Martin, A.R. Holzwarth, Biochim. Biophys. Acta 1060 (1991) 271–283.
[23] M. Werst, Y. Jia, L. Mets, G.R. Fleming, Biophys. J. 61 (1992) 868–878.
[24] G. Trinkunas, A.R. Holzwarth, Biophys. J. 66 (1994) 415–429.
[25] R. van Grondelle, J.P. Dekker, T. Gillbro, V. Sundström, Biochim. Biophys. Acta 1187 (1994) 1–65.
[26] L. Valkunas, V. Liuolia, J.P. Dekker, R. van Grondelle, Photosynth. Res. 43 (1995) 149–154.
[27] O.J.G. Somsen, L. Valkunas, R. van Grondelle, Biophys. J. 70 (1996) 669–683.
[28] A.J. Hoff, J. Amesz, in: H. Scheer (Ed.), Chlorophylls, CRC Press, Boca Raton, FL, 1991, pp. 723–738.
[29] V.V. Shubin, S.D.S. Murthy, N.V. Karapetyan, P. Mohanty, Biochim. Biophys. Acta 1060 (1991) 28–36.
[30] B.P. Wittmershaus, V.M. Woolf, W.F.J. Vermaas, Photosynth. Res. 31 (1992) 75–87.
[31] J. van der Lee, D. Bald, S.L.S. Kwa, R. van Grondelle, M. Rögner, J.P. Dekker, Photosynth. Res. 35 (1993) 311–321.
[32] S. Turconi, G. Schweitzer, A.R. Holzwarth, Photochem. Photobiol. 57 (1993) 113–119.
[33] B. Gobets, H. van Amerongen, R. Monshouwer, J. Kruip, M. Rögner, R. van Grondelle, J.P. Dekker, Biochim. Biophys. Acta 1188 (1994) 75–85.

[34] G. Hastings, L.J. Reed, S. Lin, R.E. Blankenship, Biophys. J. 69 (1995) 2044–2055.
[35] L.-O. Pålsson, J.P. Dekker, E. Schlodder, R. Monshouwer, R. van Grondelle, Photosynth. Res. 48 (1996) 239–246.
[36] J. Kruip, N.V. Karapetyan, I.V. Terekhova, M. Rögner, J. Biol. Chem. 274 (1999) 18181–18188.
[37] N.V. Karapetyan, A.R. Holzwarth, M. Rögner, FEBS Lett. 460 (1999) 395–400.
[38] B. Gobets, I.H.M. van Stokkum, M. Rögner, J. Kruip, E. Schlodder, N.V. Karapetyan, J.P. Dekker, R. van Grondelle, Biophys. J. 81 (2001) 407–424.
[39] J.M. Hayes, S. Matsuzaki, M. Rätsep, G.J. Small, J. Phys. Chem. B 104 (2000) 5625–5633.
[40] M. Rätsep, T.W. Johnson, P.R. Chitnis, G.J. Small, J. Phys. Chem. B 104 (2000) 836–847.
[41] L.-O. Pålsson, C. Flemming, B. Gobets, R. van Grondelle, J.P. Dekker, E. Schlodder, Biophys. J. 74 (1998) 2611–2622.
[42] V.V. Shubin, I.N. Bezsmertnaya, N.V. Karapetyan, FEBS Lett. 309 (1992) 340–342.
[43] A.R. Holzwarth, G. Schatz, H. Brock, E. Bittersmann, Biophys. J. 64 (1993) 1813–1826.
[44] B. Koehne, H.W. Trissl, Biochemistry 37 (1998) 5494–5500.
[45] V.V. Shubin, I.N. Bezsmertnaya, N.V. Karapetyan, J. Photochem. Photobiol. B 30 (1995) 153–160.
[46] M. Byrdin, I. Rimke, E. Schlodder, D. Stehlik, T.A. Roelofs, Biophys. J. 79 (2000) 992–1007.
[47] B. Gobets, J.T.M. Kennis, J.A. Ihalainen, M. Brazzoli, R. Croce, I.H.M van Stokkum, R. Bassi, J.P. Dekker, H. van Amerongen, G.R. Fleming, R. van Grondelle, J. Phys. Chem. B. (2001) submitted.
[48] B. Gobets, J.P. Dekker, R. van Grondelle, in: G. Garab (Ed.), Photosynthesis: Mechanisms and Effects, Vol. 1, Kluwer, Dordrecht, 1998, pp. 503–508.
[49] E.J.G. Peterman, T. Pullerits, R. van Grondelle, H. van Amerongen, J. Phys. Chem. B 101 (1997) 4448–4457.
[50] E.J.G. Peterman, S.-O. Wenk, T. Pullerits, L.-O. Pålsson, R. van Grondelle, J.P. Dekker, M. Rögner, H. van Amerongen, Biophys. J. 75 (1998) 389–398.
[51] E.J.G. Peterman, H. van Amerongen, R. van Grondelle, J.P. Dekker, Proc. Natl. Acad. Sci. USA 95 (1998) 6128–6133.
[52] I. Mukerji, K. Sauer, in: M. Baltscheffsky (Ed.), Current Research in Photosynthesis, Vol. 2, Kluwer, Dordrecht, 1990, pp. 321–324.
[53] R. van Grondelle, V. Sundström, in: H. Scheer, S. Scheider (Eds.), Photosynthetic Light-Harvesting Systems, de Gruyter, Berlin, 1988, pp. 403–438.
[54] R. van Grondelle, H. Bergström, V. Sundström, R.J. van Dorssen, M. Vos, C.N. Hunter, in: H. Scheer, S. Scheider (Eds.), Photosynthetic Light-Harvesting Systems, de Gruyter, Berlin, 1988, pp. 519–530.
[55] H.-W. Trissl, Photosynth. Res. 35 (1993) 247–263.
[56] H.-W. Trissl, C. Wilhelm, Trends Biochem. Sci. 18 (1993) 415–419.
[57] A. Rivadossi, G. Zucchelli, F.M. Garlaschi, R.C. Jennings, Photosynth. Res. 60 (1999) 209–215.
[58] G.S. Beddard, G. Porter, Nature 260 (1976) 366.
[59] S. Savikhin, D.R. Buck, W.S. Struve, R.E. Blankenship, A.S. Taisova, V.I. Novoderezhkin, Z.G. Fetisova, FEBS Lett. 430 (1998) 323–326.
[60] L. Valkunas, G. Trinkunas, V. Liuolia, R. van Grondelle, Biophys. J. 69 (1995) 1117–1129.
[61] R. van Grondelle, Biochim. Biophys. Acta 811 (1985) 147–195.
[62] M. Werst, Y.W. Jia, L. Mets, G.R. Fleming, Biophys. J. 61 (1992) 868–878.
[63] L.-O. Pålsson, S.E. Tjus, B. Andersson, T. Gillbro, Chem. Phys. 194 (1995) 291–302.
[64] S. Savikhin, W. Xu, V. Soukoulis, P.R. Chitnis, W.S. Struve, Biophys. J. 76 (1999) 3278–3288.
[65] A.N. Melkozernov, S. Lin, R.E. Blankenship, Biochemistry 39 (2000) 1489–1498.
[66] G. Hastings, F.A.M. Kleinherenbrink, S. Lin, R.E. Blankenship, Biochemistry 33 (1994) 3185–3192.
[67] S. Kumazaki, H. Kandori, H. Petek, K. Yoshihara, I. Ikegami, J. Phys. Chem. 98 (1994) 10335–10342.
[68] S. Kumazaki, I. Ikegami, H. Furusawa, S. Yasuda, K. Yoshihara, J. Phys. Chem. B 105 (2001) 1093–1099.
[69] N.V. Karapetyan, D. Dorra, G. Schweitzer, I.N. Bezsmertnaya, A.R. Holzwarth, Biochemistry 36 (1997) 13830–13837.
[70] M. Du, X. Xie, Y. Jia, L. Mets, G.R. Fleming, Chem. Phys. Lett. 201 (1993) 535–542.
[71] J.T.M. Kennis, B. Gobets, I.H.M. van Stokkum, J.P. Dekker, R. van Grondelle, G.R. Fleming, J. Phys. Chem. B 105 (2001) 4485–4494.
[72] B. Gobets, I.H.M. van Stokkum, F. van Mourik, M. Rögner, J. Kruip, J.P. Dekker, R. van Grondelle, in: G. Garab (Ed.), Photosynthesis: Mechanisms and Effects, Vol. 1, Kluwer, Dordrecht, 1998, pp. 571–574.
[73] G. Trinkunas, A.R. Holzwarth, Biophys. J. 71 (1996) 351–364.
[74] G.F.W. Searle, R. Tamkivi, A. van Hoek, T.J. Schaafsma, J. Chem. Soc. Faraday Trans. 2 (84) (1988) 315–327.
[75] B.P. Wittmershaus, in: J. Biggins (Ed.), Progress in Photosynthesis Research, Martinus Nijhoff, Dordrecht, 1987, pp. 75–82.
[76] B.P. Wittmershaus, D.S. Berns, C. Huang, Biophys. J. 52 (1987) 829–836.
[77] R.A. Friesner, Y.D. Won, Biochim. Biophys. Acta 977 (1989) 99–122.
[78] P.D. Laible, W. Zipfel, T.G. Owens, Biophys. J. 66 (1994) 844–860.
[79] N.T.H. White, G.S. Beddard, J.R.G. Thorne, T.M. Feehan, T.E. Keyes, P. Heathcote, J. Phys. Chem. 100 (1996) 12086–12099.
[80] G.S. Beddard, Phil. Trans. R. Soc. London A 356 (1998) 421–448.
[81] R.J.W. Louwe, J. Vrieze, A.J. Hoff, T.J. Aartsma, J. Phys. Chem. B 101 (1997) 11280–11287.
[82] S. Savikhin, D.R. Buck, W.S. Struve, in: D.L. Andrews, A.A. Demidov (Eds.), Resonance Energy Transfer, John Wiley and Sons, New York, 1999, pp. 399–434.
[83] C.C. Gradinaru, S. Ozdemir, D. Gulen, I.H.M. van Stok-

kum, R. van Grondelle, H. van Amerongen, Biophys. J. 75 (1998) 3064–3077.
[84] R.M. Pearlstein, Photochem. Photobiol. 35 (1982) 835–844.
[85] S.P. Kudzmauskas, L.L. Valkunas, A.Y. Borisov, J. Theor. Biol. 105 (1983) 13–23.
[86] W.T.F. den Hollander, J.G.C. Bakker, R. van Grondelle, Biochim. Biophys. Acta 725 (1983) 492–507.
[87] O.J.G. Somsen, F. van Mourik, R. van Grondelle, L. Valkunas, Biophys. J. 66 (1994) 1580–1596.
[88] W.W. Parson, in: H. Scheer (Ed.), Chlorophylls, CRC Press, Boca Raton, FL, 1991, pp. 1153–1180.
[89] M.L. Groot, F. van Mourik, C. Eijckelhoff, I.H.M. van Stokkum, J.P. Dekker, R. van Grondelle, Proc. Natl. Acad. Sci. USA 94 (1997) 4389–4394.
[90] J.R. Durrant, D.R. Klug, S.L.S. Kwa, R. van Grondelle, G. Porter, J.P. Dekker, Proc. Natl. Acad. Sci. USA 92 (1995) 4798–4802.
[91] G.S. Beddard, J. Phys. Chem. B 102 (1998) 10966–10973.
[92] M.E. van Brederode, R. van Grondelle, FEBS Lett. 455 (1999) 1–7.
[93] M.E. van Brederode, I.H.M. van Stokkum, E. Katilius, F. van Mourik, M.R. Jones, R. van Grondelle, Biochemistry 38 (1999) 9556–9556.
[94] M.E. van Brederode, F. van Mourik, I.H.M. van Stokkum, M.R. Jones, R. van Grondelle, Proc. Natl. Acad. Sci. USA 96 (1999) 2054–2059.
[95] S. Neerken, K.A. Schmidt, T.J. Aartsma, J. Amesz, Biochemistry 38 (1999) 13216–13222.
[96] S. Neerken, T.J. Aartsma, J. Amesz, Biochemistry 39 (2000) 3297–3303.
[97] R. Croce, D. Dorra, A.R. Holzwarth, R.C. Jennings, Biochemistry 39 (2000) 6341–6348.